Chapter 4

Intrinsic Defects and Defect Concentrations in $MgAl_2O_4$ Spinel

4.1 Introduction

$MgAl_2O_4$ spinel is an important industrial ceramic with a range of applications that take advantage of its refractory and radiation tolerance properties [39]. Such materials will contain lattice defects which will influence their mechanical and optical properties. This is particularly relevant when used within radioactive environments, as bombardment by ionising radiation will lead to elevated defect concentrations.

The structure of normal spinel was shown in figure 3.1. If the O^{2-} ions are considered to form a face centred array, within the unit cell, Mg^{2+} ions occupy tetrahedral interstices between O^{2-} ions, the smaller Al^{3+} ions are sited in octahedral interstices. These cation sublattices only partly fill the available interstices and the remaining positions are generally considered to accommodate interstitial ions [114]. As we shall see, however, the structure of the interstitial species can be more complex then assumed in such a simple model.

A second simplification that has been made in the above description of spinel is that all 8a tetrahedral sites are occupied by Mg^{2+} and all 16d octahedral sites are occupied by Al^{3+}. As was shown in chapter 3 there is a degree of disorder between the two sites so that some tetrahedral sites are occupied by Al^{3+} ions and some octahedral sites are occupied by Mg^{2+} ions. The cation disorder process can be described using the following equation:

$$Mg^{\times}_{Mg} + Al^{\times}_{Al} \rightarrow Mg'_{Al} + Al^{\cdot}_{Mg} \tag{4.1}$$

where, for example, $Al^{\times}_{Al}$ indicates an Al^{3+} ion at an octahedral 16d site and $Al^{\cdot}_{Mg}$ indicates an Al^{3+} ion at a tetrahedral 8a site. Since the 8a site is occupied, in a perfect normal spinel, by Mg^{2+}, the substitution of an Al^{3+} ion results in charge disparity of positive one. The value of i also depends on processing conditions, temperature and pressure but values between $0.05 \leq i \leq 0.33$ are generally accepted [97]. In this study we use computer simulation (in particular the CASCADE code [121]) to investigate the structure of isolated and clustered intrinsic defects and obtain an estimate of their

relative formation energies.

4.1.1 Mass Action Analysis

A recent paper by Smith *et al.* [108] predicted the residual defects formed by collision cascades in $MgAl_2O_4$ spinel. Using the Mott-Littleton approach as described in section 2.7 the structure and formation enthalpies of these defects have been calculated and are presented in this chapter. As well as the energies associated with the different intrinsic defect processes.

These enthalpies are used in conjunction with a complete set of mass action equations [133, 134] to calculate defect concentrations for spinel. These mass action equations are solved simultaneously using Newtons method in 2D (discussed along with other techniques by Broyden [135]). The iterative process is terminated once the variation in defect concentrations between consecutive cycles is less than 10^{-18}.

Defect association reactions were discussed in section 1.1.3 these form the basis of the analysis used in sections 4.2.1 and 4.2.2 of this chapter. Mass action analysis [133, 134] relates the energy associated with a given defect equilibrium to the relevant equilibrium defect concentrations. As an example, the mass action equation associated with the antisite reaction (equation 4.1) is of the form,

$$[\mathrm{Mg}'_{\mathrm{Al}}][\mathrm{Al}^{\cdot}_{\mathrm{Mg}}] = \exp\left(-\frac{H_{equ4.1}}{kT}\right) \tag{4.2}$$

where $\Delta H_{equ4.1}$ is the predicted internal energy of equation 4.1, k is Boltz-

mann's constant and T, the temperature. Provided that this reaction is the dominant means of forming both the Mg'_{Al} and $Al^{\cdot}_{Mg}$ defects in $MgAl_2O_4$ then electroneutrality requires that,

$$[Mg'_{Al}] = [Al^{\cdot}_{Mg}] \tag{4.3}$$

combining equations 4.2 and 4.3 yields an expression for the concentrations of each constituent defect type, these are, for Mg'_{Al},

$$[Mg'_{Al}] = \exp\left(-\frac{H_{equ4.1}}{2kT}\right) \tag{4.4}$$

and for $Al^{\cdot}_{Mg}$,

$$[Al^{\cdot}_{Mg}] = \exp\left(-\frac{H_{equ4.1}}{2kT}\right) \tag{4.5}$$

There are some approximations associated with this type of calculations. First, the energy calculated for equation 4.1 relies on the point defect model, in real ceramics defects are able to interact in such a way as to reduce the total energy of the system. This implies that the real concentrations will be higher than those calculated. Second, there are many competing processes associated with the concentrations of defects in a solid, thus while equation 4.1 may be the dominant reaction concerning the formation of Mg'_{Al} and $Al^{\cdot}_{Mg}$ defects the actual concentrations will depend on how these defects interact with all other defect species within the lattice. In order to eliminate this problem a set of equilibria may be solved simultaneously in such a way as to

provide an internally consistent set of concentrations.

As with almost all calculations relying on a full charge model the defect energies calculated here will tend to overestimate the real values. This in turn means that calculated concentrations will be lower than implied by experiment.

4.2 Intrinsic Defects

4.2.1 Isolated Defects

There are five distinct defect equilibria associated with the formation of intrinsic defects in $MgAl_2O_4$ these comprise the antisite process, equation 4.1, the magnesium, aluminium and oxygen Frenkel processes, equations 4.6 - 4.8 and the Schottky process, equation 4.9.

$$\mathrm{Mg}_{\mathrm{Mg}}^{\times} \rightleftharpoons \mathrm{Mg}_{i}^{\cdot\cdot} + \mathrm{V}_{\mathrm{Mg}}^{\prime\prime} \tag{4.6}$$

$$\mathrm{Al}_{\mathrm{Al}}^{\times} \rightleftharpoons \mathrm{Al}_{i}^{\cdot\cdot\cdot} + \mathrm{V}_{\mathrm{Al}}^{\prime\prime\prime} \tag{4.7}$$

$$\mathrm{O}_{\mathrm{O}}^{\times} \rightleftharpoons \mathrm{O}_{i}^{\prime\prime} + \mathrm{V}_{\mathrm{O}}^{\cdot\cdot} \tag{4.8}$$

$$\mathrm{Mg}_{\mathrm{Mg}}^{\times} + 2\mathrm{Al}_{\mathrm{Al}}^{\times} + 4\mathrm{O}_{\mathrm{O}}^{\times} \rightleftharpoons \mathrm{V}_{\mathrm{Mg}}^{\prime\prime} + 2\mathrm{V}_{\mathrm{Al}}^{\prime\prime\prime} + 4\mathrm{V}_{\mathrm{O}}^{\cdot\cdot} + \mathrm{MgAl_2O_4} \tag{4.9}$$

Table 4.1 displays the calculated defect energies for isolated defects in $MgAl_2O_4$. These comprise cation and anion vacancies and interstitials as well as cation antisite defects.

Table 4.1: Isolated defect energies (eV) in $MgAl_2O_4$, with and without shells (note the interstitial ions have split configurations).

Species	Energy with shells	Energy without shells
$V_O^{\cdot\cdot}$	25.00	25.48
V''_{Mg}	26.70	28.09
V'''_{Al}	56.49	57.00
O''_i	-14.01	-12.99
$Mg_i^{\cdot\cdot}$	-15.78	-15.72
$Al_i^{\cdot\cdot\cdot}$	-42.64	-41.91
$Al_{Mg}^{\cdot}$	-28.53	-28.40
Mg'_{Al}	29.99	29.94

It might be expected that the cation interstitial ions would lie at the unoccupied 8b interstices, however, recent molecular dynamics calculations by Smith *et al.* [108] suggest that the interstitials have more complex split structures: oxygen is found to form a split $O''_i - V_O^{\cdot\cdot} - O''_i$ complex aligned along $\langle 1\bar{1}0\rangle$ (figure 4.1), similarly magnesium forms a split $Mg_i^{\cdot\cdot} - V''_{Mg} - Mg_i^{\cdot\cdot}$ complex also along either $\langle 110\rangle$ or $\langle 1\bar{1}0\rangle$ (figure 4.2) depending on the local oxygen positions. Aluminium does not form a split configuration about an octahedral site, however an $Al_i^{\cdot\cdot\cdot} - V''_{Mg} - Mg_i^{\cdot\cdot}$ complex (figure 4.3), with an Al^{3+} ion taking the place of one Mg^{2+} ion in the magnesium split cluster, is stable and energetically favoured compared to an isolated interstitial Al^{3+} at an unoccupied tetrahedral interstice. As with the magnesium case interstitials form in both $\langle 110\rangle$ or $\langle 1\bar{1}0\rangle$ directions, but as the two ions are no longer iden-

tical there are additionally distinct splits in $\langle\bar{1}\bar{1}0\rangle$ and $\langle\bar{1}10\rangle$ directions. As a convention, the directions for this split structure will refer to the direction from the magnesium to the aluminium ion throughout.

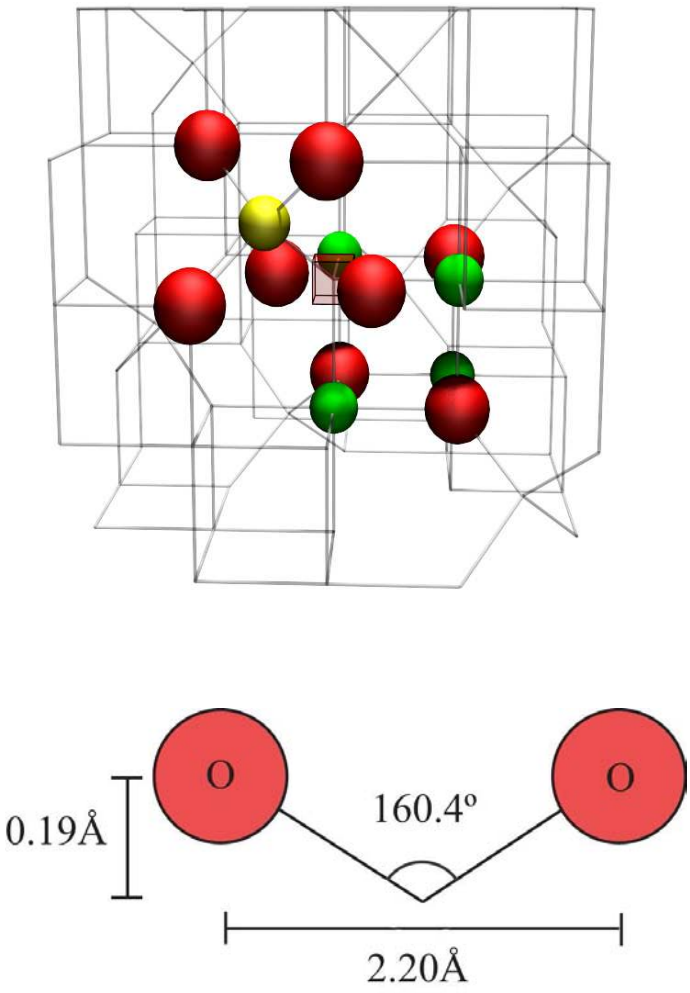

Figure 4.1: Two diagrams showing the structure of the $O_i'' - V_O^{\cdot\cdot} - O_i''$ split oxygen interstitial. The now vacant oxygen site is indicated in the upper diagram by the transparent red cube and it is from this perfect lattice point that the angle between the two oxygen ions is measured in the lower diagram.

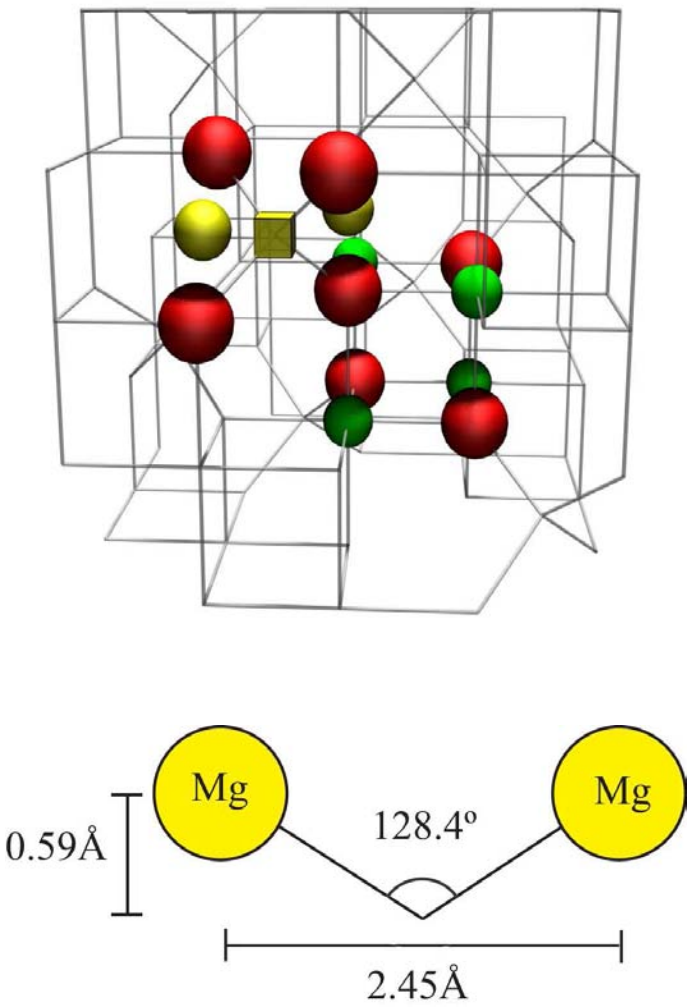

Figure 4.2: Two diagrams showing the structure of the $Mg_i^{\cdot\cdot} - V''_{Mg} - Mg_i^{\cdot\cdot}$ split magnesium interstitial. The now vacant magnesium site is indicated in the upper diagram by the transparent yellow cube and it is from this point that the angle between the two magnesium ions is measured in the lower diagram.

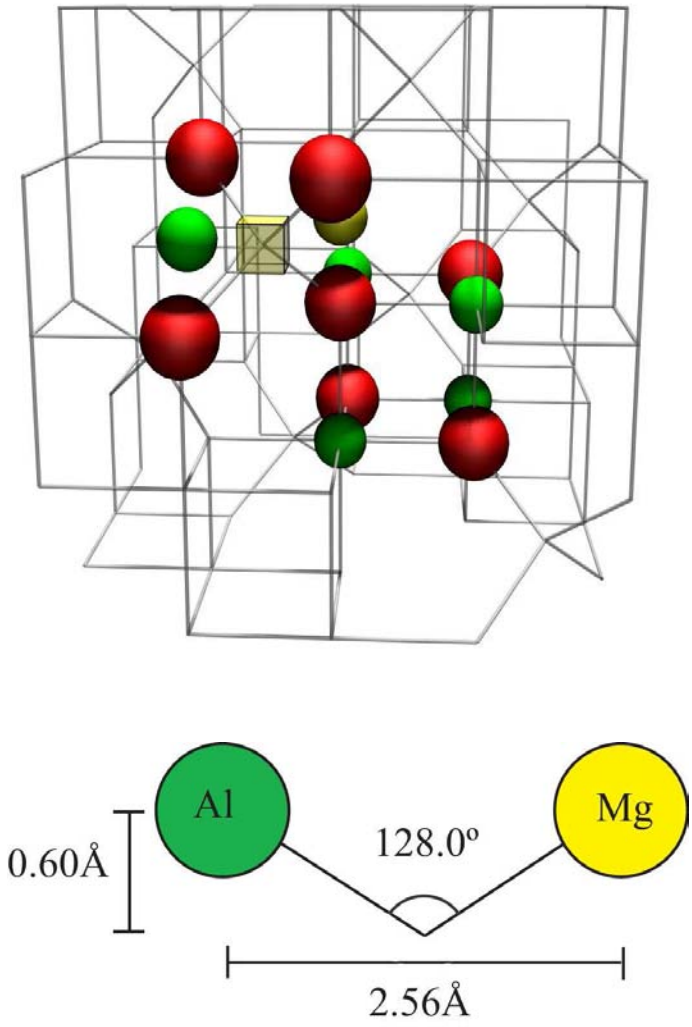

Figure 4.3: Two diagrams showing the structure of the $Al_i^{\cdots} - V''_{Mg} - Mg_i^{\cdot\cdot}$ split aluminium interstitial. Note how the Al^{3+} interstitial has displaced a lattice Mg^{2+} ion into an adjacent interstitial site leaving behind a vacant tetrahedral site (as in figure 4.2)

.

Using the energies reported in table 4.1 we can predict the energies for equations 4.1 - 4.9, these are as reported in table 4.2 and have been normalised

per defect formed.

Table 4.2: Normalised defect energies (eV) for intrinsic defect processes, isolated defects, with and without shells.

Process	Defect energy (shells)	Defect energy (no shells)
Schottky	5.32	5.99
O Frenkel	5.50	6.25
Mg Frenkel	5.46	6.19
Al Frenkel	6.93	7.55
Cation antisite	0.73	0.77
$Mg_i^{\cdot\cdot} + V_{Al}''' + Al_{Mg}^{\cdot}$	5.73	6.05
$Al_i^{\cdot\cdot\cdot} + V_{Mg}'' + Mg_{Al}'$	6.66	7.68

Chapter 3 focused on cation disorder on the assumption that cation disorder is by far the most common type of defect in the $MgAl_2O_4$ lattice. Table 4.2 confirms that we predict this to be the case.

While antisite disorder is found to be much more common than other types the Schottky, oxygen Frenkel and magnesium Frenkel disorder energies are sufficiently close that this simulation technique is unable to differentiate between them. This picture is similar to calculations cited by Chiang *et al.* [136] which suggest energies in the range 4.5 - 7eV. Energies derived from diffusion data seem, however, to predict lower values, 3.74eV for V_{Mg}'' diffusion [137], 4.55±0.69 eV for oxygen diffusion [138] and 2.0-3.2eV for Frenkel defect formation [139]. These numbers are substantially lower than those predicted through isolated defect formation, especially as the diffusion numbers contain

not only the defect formation energy but also the defect migration energy (as was discussed in section 1.1.4).

As it is relatively energetically favourable to form antisite defects, the following equilibria should be considered (equations 4.10 - 4.13). In each case, we are considering how defects formed through Schottky or Frenkel equilibria interact with existing cation antisite defects.

$$V'''_{Al} + Al^{\cdot}_{Mg} \rightleftharpoons Al^{\times}_{Al} + V''_{Mg} \tag{4.10}$$

$$V''_{Mg} + Mg'_{Al} \rightleftharpoons Mg^{\times}_{Mg} + V'''_{Al} \tag{4.11}$$

$$Mg^{\cdot\cdot}_{i} + Al^{\cdot}_{Mg} \rightleftharpoons Mg^{\times}_{Mg} + Al^{\cdot\cdot\cdot}_{i} \tag{4.12}$$

$$Al^{\cdot\cdot\cdot}_{i} + Mg'_{Al} \rightleftharpoons Al^{\times}_{Al} + Mg^{\cdot\cdot}_{i} \tag{4.13}$$

Formation energies on the left hand sides of equations 4.10 - 4.13 are listed in table 4.3 (it is stressed that these numbers are simply the sum of the relevant energies listed in table 4.1 rather than the energy of a cluster comprised of those defects). Interestingly a combination of isolated $Mg^{\cdot\cdot}_{i}$ and $Al^{\cdot}_{Mg}$ defects is lower in energy than an $Al^{\cdot\cdot\cdot}_{i}$ (i.e. the left hand side of equation 4.12 is prefered over the right hand side).

To determine if reaction 4.12 will yield a significant defect population of $Mg^{\cdot\cdot}_{i}$ the following mass action equation should be considered

$$\frac{[Al^{\cdot\cdot\cdot}_{i}]}{[Mg^{\cdot\cdot}_{i}][Al^{\cdot}_{Mg}]} = \exp\left(-\frac{\Delta H}{kT}\right) \tag{4.14}$$

Table 4.3: Combinations of isolated defect energies (eV), examples are for calculation with shells on the O^{2-} ions.

Species	Energy	Internal energies (Eq. 4.10 - 4.13)	Equivalent species
$V'''_{Al} + Al^{\cdot}_{Mg}$	27.96	1.26	V''_{Mg}
$V''_{Mg} + Mg'_{Al}$	56.69	0.20	V'''_{Al}
$Mg^{\cdot\cdot}_{i} + Al^{\cdot}_{Mg}$	-44.31	-1.67	$Al^{\cdot\cdot\cdot}_{i}$
$Al^{\cdot\cdot\cdot}_{i} + Mg'_{Al}$	-12.65	3.13	$Mg^{\cdot\cdot}_{i}$

where $\Delta H = 1.67$ eV (with shells). However, $[\,Al^{\cdot}_{Mg}]$ is controlled by the antisite reaction (equation 4.1). Thus,

$$[Mg'_{Al}] = [Al^{\cdot}_{Mg}] = \exp\left(\frac{-0.73}{kT}\right) \tag{4.15}$$

Combining this with equation 4.14 gives

$$[Al^{\cdot\cdot\cdot}_{i}] = [Mg^{\cdot\cdot}_{i}] \exp\left(\frac{-0.94}{kT}\right) \tag{4.16}$$

Thus the concentration of $Al^{\cdot\cdot\cdot}_{i}$ is clearly depreciated with respect to $[Mg^{\cdot\cdot}_{i}]$. If we follow the equilibria for equation 4.13 it leads to the same numerical conclusion.

The two vacancy reactions are also coupled through the cation antisite reaction. Consequently, in both cases, using equation 4.11 we find,

$$\frac{[V''_{Mg}][Mg'_{Al}]}{[V'''_{Al}]} = \exp\left(\frac{0.2}{kT}\right) \tag{4.17}$$

and through the cation antisite reaction,

$$[V''_{Mg}] = [V'''_{Al}] \exp\left(\frac{0.93}{kT}\right) \tag{4.18}$$

Thus the cation antisite equilibrium leads to the conclusion that the V''_{Mg} concentration is substantially greater than the V'''_{Al} concentration.

The relations 4.10 - 4.13 suggest some other possible intrinsic reactions,

$$Mg^{\times}_{Mg} + Al^{\times}_{Al} \rightleftharpoons Mg^{\cdot\cdot}_{i} + V'''_{Al} + Al^{\cdot}_{Mg} \tag{4.19}$$

$$Mg^{\times}_{Mg} + Al^{\times}_{Al} \rightleftharpoons Al^{\cdot\cdot\cdot}_{i} + V''_{Mg} + Mg'_{Al} \tag{4.20}$$

The energies for these process can be obtained in a similar way to that used for equations 4.10 - 4.13. Equation 4.19 corresponds to the following equilibrium,

$$[V'''_{Al}][Mg^{\cdot\cdot}_{i}][Al^{\cdot}_{Mg}] = \exp\left(\frac{-12.18}{kT}\right) \tag{4.21}$$

combining this with equation 4.15 yields,

$$[V'''_{Al}] = [Mg^{\cdot\cdot}_{i}] = \exp\left(\frac{-5.73}{kT}\right) \tag{4.22}$$

Both these processes are similar in energy to the Frenkel reactions they replace, Al'''_i formation via equation 4.20 being marginally lower than via its Frenkel reaction (equation 4.7).

Additionally it is possible for a 'partial Schottky' reaction to occur, in which a formula unit of either MgO or Al_2O_3 is formed. The energies of these processes are presented in table 4.4 and are similar in magnitude to the Schottky and oxygen/magnesium Frenkel reactions discussed previously.

Table 4.4: Normalised formation energies (eV) for a singular formular unit of MgO and Al_2O_3 via 'partial Schottky' assuming isolated defect formation, with and without shells.

Process	Per defect energy (shells)	Per defect energy (no shells)
MgO formation	5.26	6.20
Al_2O_3 formation	5.46	5.96

Mass Action Calculations

Ignoring the possibility of defect clustering there are, in $MgAl_2O_4$ spinel, eight distinct defect species comprising, three vacancies, the three corresponding interstitials and the two cation antisite species. In order to solve simultaneously for the concentrations a minimum of eight equations are required. Seven of these (equations 4.23-4.29) are mass action equations corresponding to the intrinsic defect reactions, equations 4.1-4.9 and 4.10-4.13. The final equation arises out of requiring electroneutrality for the system be maintained. In practice this requires setting $Z^+ \equiv Z^-$ in equations 4.30 and 4.31. It was found that this series of equations is not sufficient to ensure that vacancies (subtracting those arising from Frenkel defects) are created in such a way as to maintain stoichiometry between anion and the two cation species, hence an additional condition, equation 4.32 was imposed.

$$[\mathrm{Mg}'_{Al}][\mathrm{Al}^{\cdot}_{Mg}] = \exp\left(\frac{-H_{eqn4.1}}{kT}\right) \tag{4.23}$$

$$[\mathrm{Mg}_i^{\cdot\cdot}][\mathrm{V}''_{Mg}] = \exp\left(\frac{-H_{eqn4.6}}{kT}\right) \tag{4.24}$$

$$[\mathrm{Al}_i^{\cdot\cdot\cdot}][\mathrm{V}'''_{Mg}] = \exp\left(\frac{-H_{eqn4.7}}{kT}\right) \tag{4.25}$$

$$[\mathrm{V}_O^{\cdot\cdot}][\mathrm{O}''_i] = \exp\left(\frac{-H_{eqn4.8}}{kT}\right) \tag{4.26}$$

$$[\mathrm{V}''_{\mathrm{Mg}}]\ [\mathrm{V}'''_{\mathrm{Al}}]^2[\mathrm{V}_{\mathrm{O}}^{\cdot\cdot}]^4 = \exp\left(\frac{-H_{eqn4.9}}{kT}\right) \tag{4.27}$$

$$\frac{[V''_{Mg}]}{[V'''_{Al}][Al_{Mg}^{\cdot}]} + \frac{[Al_i^{\cdot\cdot\cdot}]}{[Mg_i^{\cdot\cdot}][Al_{Mg}^{\cdot}]} = \exp\left(\frac{-H_{eqn4.10}}{kT}\right) + \exp\left(\frac{-H_{eqn4.12}}{kT}\right) \tag{4.28}$$

$$\frac{[V'''_{Al}]}{[V''_{Mg}][Mg'_{Al}]} + \frac{[Mg_i^{\cdot\cdot}]}{[Al_i^{\cdot\cdot\cdot}][Mg'_{Al}]} = \exp\left(\frac{-H_{eqn4.11}}{kT}\right) + \exp\left(\frac{-H_{eqn4.13}}{kT}\right) \tag{4.29}$$

$$\mathrm{Z}^+ = 3[\mathrm{Al}_{\mathrm{i}}^{\cdot\cdot\cdot}] + 2[\mathrm{Mg}_{\mathrm{i}}^{\cdot\cdot}] + 2[\mathrm{V}_{\mathrm{O}}^{\cdot\cdot}] + [\mathrm{Al}_{\mathrm{Mg}}^{\cdot}] \tag{4.30}$$

$$\mathrm{Z}^- = 3[\mathrm{V}'''_{\mathrm{Al}}] + 2[\mathrm{V}''_{\mathrm{Mg}}] + 2[\mathrm{O}''_{\mathrm{i}}] + [\mathrm{Mg}'_{\mathrm{Al}}] \tag{4.31}$$

$$[\mathrm{V}_{\mathrm{O}}^{\cdot\cdot}] - [\mathrm{O}''_{\mathrm{i}}] = \frac{4}{3}\left([\mathrm{V}'''_{\mathrm{Al}}] + [\mathrm{V}''_{\mathrm{Mg}}] - [\mathrm{Al}_{\mathrm{i}}^{\cdot\cdot\cdot}] - [\mathrm{Mg}_{\mathrm{i}}^{\cdot\cdot}]\right) \tag{4.32}$$

The results of solving these equations are shown in figure 4.4 for temperatures in the range 1000K-2000K. The dominance of the two antisite defects is immediately obvious, their concentrations throughout the range being more than 10 orders of magnitude higher than those of any other defect. Of the remaining defect species the vacancies are somewhat (or in the case of V'''_{Al}, greatly) more numerous than their respective interstitials. This is expected as table 4.2 shows the Schottky process to be favoured with respect to the anion and cation Frenkel reactions. Though not discernable on the scale of figure 4.4 the concentrations of the two antisite defects are not equal. $[Mg'_{Al}]$ is depleted slightly with respect to $[Al^{\cdot}_{Mg}]$ indicating that equations 4.28 and 4.29 are having a measurable effect on the calculation. These processes also provide a likely explanation for the $[V''_{Mg}]$ being calculated to be higher than that of the $[V'''_{Al}]$ contrary to what might be expected from consideration of the Schottky process alone.

4.2.2 Clustered Defects

While isolated defects may provide a good approximation to defect equilibria at low defect concentrations, at high defect concentrations oppositely charged defects species will form locally charge compensating cluster configurations.

The huge concentrations of antisite defects relative to the various interstitial and vacancy species force us to consider an interesting assumption; that these antisites are so common in the lattice that all interstial and vacancy defects inevitably form charge compensated clusters where it is an energet-

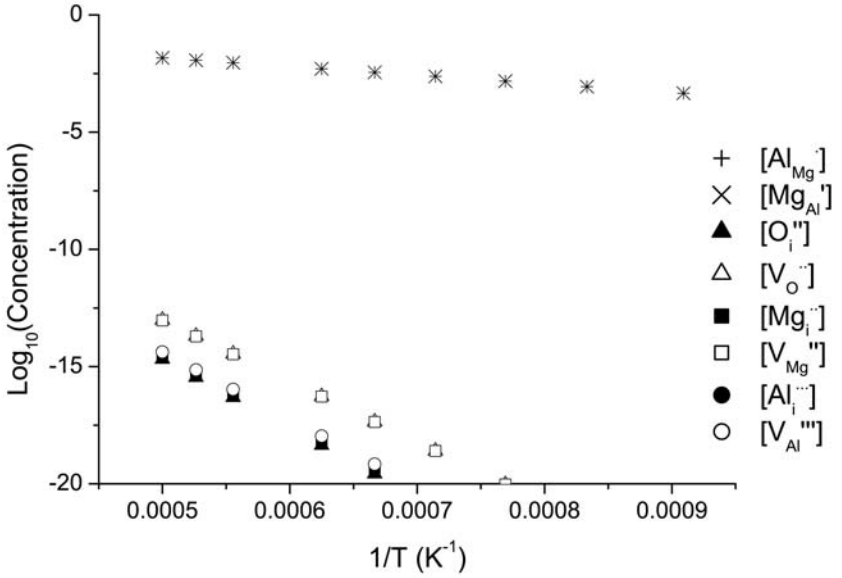

Figure 4.4: Intrinsic defect concentrations for $MgAl_2O_4$ spinel for temperatures in the range 1000K-2000K.

ically favourable process, i.e. that configurational entropy will not have a significant role in determining the extent of cluster formation.

Table 4.5 shows the calculated absolute and binding energies for clusters consisting of a single vacancy (or interstitial) defect with a number of the oppositely charged antisite defects. For each vacancy and/or interstitial species the highest binding energy per defect is for the trimer defect. This is the neutral cluster in the case of oxygen and magnesium vacancies and interstials but singly charged in the aluminium defect containing clusters. For each cluster all first and second neighbour geometric configurations were investigated, where a second neighbour configuration was lower in energy the binding energies for third neighbour configurations were also studied.

Table 4.5: Cluster defect and binding energies (BE) (eV), with and without shells. Negative binding energy equates to a bound cluster.

Cluster	Energy (shells)	BE (shells)	Energy	BE
$\{V_O^{\cdot\cdot}:Mg'_{Al}\}^{\cdot}$	53.43	-1.55	53.58	-1.85
$\{V_O^{\cdot\cdot}:2Mg'_{Al}\}^{\times}$	82.48	-4.19	82.94	-2.42
$\{V''_{Mg}:Al^{\cdot}_{Mg}\}'$	-2.57	-0.74	-1.21	-0.90
$\{V''_{Mg}:2Al^{\cdot}_{Mg}\}^{\times}$	-32.13	-1.41	-30.02	-1.30
$\{V'''_{Al}:Al^{\cdot}_{Mg}\}''$	26.27	-1.39	26.87	-1.72
$\{V'''_{Al}:2Al^{\cdot}_{Mg}\}'$	-3.17	-2.60	-3.01	-3.20
$\{V'''_{Al}:3Al^{\cdot}_{Mg}\}^{\times}$	-32.39	-3.29	-32.36	-4.15
$\{O''_i:Al^{\cdot}_{Mg}\}'$	-44.26	-1.73	-43.75	-2.35
$\{O''_i:2Al^{\cdot}_{Mg}\}^{\times}$	-73.76	-2.70	-73.59	-4.57
$\{Mg_i^{\cdot\cdot}:Mg'_{Al}\}^{\cdot}$	13.18	-1.03	13.05	-1.17
$\{Mg_i^{\cdot\cdot}:2Mg'_{Al}\}^{\times}$	42.42	-1.77	42.06	-2.10
$\{Al_i^{\cdot\cdot\cdot}:Mg'_{Al}\}^{\cdot\cdot}$	-14.16	-1.51	-13.67	-1.70
$\{Al_i^{\cdot\cdot\cdot}:2Mg'_{Al}\}^{\cdot}$	14.89	-2.45	15.03	-2.94
$\{Al_i^{\cdot\cdot\cdot}:3Mg'_{Al}\}^{\times}$	44.44	-2.88	44.52	-3.39
$\{Mg'_{Al}:Al^{\cdot}_{Mg}\}^{\times}$	0.98	-0.48	0.94	-0.60

Considering the trimer defects we can propose a series of reactions analagous to the Frenkel and Schottky processes these are equations 4.33 - 4.36:

$$2\mathrm{Mg}'_{\mathrm{Al}} + 2\mathrm{Al}^{\cdot}_{\mathrm{Mg}} + \mathrm{Mg}^{\times}_{Mg} \rightleftharpoons \{\mathrm{Mg}^{\cdot\cdot}_{\mathrm{i}}{:}2\mathrm{Mg}'_{\mathrm{Al}}\}^{\times} + \{\mathrm{V}''_{\mathrm{Mg}}{:}2\mathrm{Al}^{\cdot}_{\mathrm{Mg}}\}^{\times} \tag{4.33}$$

$$2\mathrm{Mg}'_{\mathrm{Al}} + 2\mathrm{Al}^{\cdot}_{\mathrm{Mg}} + \mathrm{Al}^{\times}_{Al} \rightleftharpoons \{\mathrm{Al}^{\cdot\cdot\cdot}_{\mathrm{i}}{:}2\mathrm{Mg}'_{\mathrm{Al}}\}^{\cdot} + \{\mathrm{V}'''_{\mathrm{Al}}{:}2\mathrm{Al}^{\cdot}_{\mathrm{Mg}}\}' \tag{4.34}$$

$$2\mathrm{Mg}'_{\mathrm{Al}} + 2\mathrm{Al}^{\cdot}_{\mathrm{Mg}} + \mathrm{O}^{\times}_{O} \rightleftharpoons \{\mathrm{O}''_{\mathrm{i}}{:}2\mathrm{Al}^{\cdot}_{\mathrm{Mg}}\}^{\times} + \{\mathrm{V}^{\cdot\cdot}_{\mathrm{O}}{:}2\mathrm{Mg}'_{\mathrm{Al}}\}^{\times} \tag{4.35}$$

$$\begin{aligned} 8\mathrm{Mg}'_{\mathrm{Al}} + 6\mathrm{Al}^{\cdot}_{\mathrm{Mg}} + \mathrm{Mg}^{\times}_{Mg} + 2\mathrm{Al}^{\times}_{Al} + 4\mathrm{O}^{\times}_{O} \rightleftharpoons \{\mathrm{V}''_{\mathrm{Mg}}{:}2\mathrm{Al}^{\cdot}_{\mathrm{Mg}}\}^{\times} + \\ 2\{\mathrm{V}'''_{\mathrm{Al}}{:}2\mathrm{Al}^{\cdot}_{\mathrm{Mg}}\}' + 4\{\mathrm{V}^{\cdot\cdot}_{\mathrm{O}}{:}2\mathrm{Mg}'_{\mathrm{Al}}\}^{\times} + \mathrm{MgAl_2O_4} \end{aligned} \tag{4.36}$$

Similarly for the dimer defects:

$$\mathrm{Mg}'_{\mathrm{Al}} + \mathrm{Al}^{\cdot}_{\mathrm{Mg}} + \mathrm{Mg}^{\times}_{Mg} \rightleftharpoons \{\mathrm{Mg}^{\cdot\cdot}_{\mathrm{i}}{:}\mathrm{Mg}'_{\mathrm{Al}}\}^{\cdot} + \{\mathrm{V}''_{\mathrm{Mg}}{:}\mathrm{Al}^{\cdot}_{\mathrm{Mg}}\}' \tag{4.37}$$

$$\mathrm{Mg}'_{\mathrm{Al}} + \mathrm{Al}^{\cdot}_{\mathrm{Mg}} + \mathrm{Al}^{\times}_{Al} \rightleftharpoons \{\mathrm{Al}^{\cdot\cdot\cdot}_{\mathrm{i}}{:}\mathrm{Mg}'_{\mathrm{Al}}\}^{\cdot\cdot} + \{\mathrm{V}'''_{\mathrm{Al}}{:}\mathrm{Al}^{\cdot}_{\mathrm{Mg}}\}'' \tag{4.38}$$

$$\mathrm{Mg}'_{\mathrm{Al}} + \mathrm{Al}^{\cdot}_{\mathrm{Mg}} + \mathrm{O}^{\times}_{O} \rightleftharpoons \{\mathrm{O}''_{\mathrm{i}}{:}\mathrm{Al}^{\cdot}_{\mathrm{Mg}}\}' + \{\mathrm{V}^{\cdot\cdot}_{\mathrm{O}}{:}\mathrm{Mg}'_{\mathrm{Al}}\}^{\cdot} \tag{4.39}$$

$$\begin{aligned} 4\mathrm{Mg}'_{\mathrm{Al}} + 3\mathrm{Al}^{\cdot}_{\mathrm{Mg}} + \mathrm{Mg}^{\times}_{Mg} + 2\mathrm{Al}^{\times}_{Al} + 4\mathrm{O}^{\times}_{O} \rightleftharpoons \{\mathrm{V}''_{\mathrm{Mg}}{:}\mathrm{Al}^{\cdot}_{\mathrm{Mg}}\}' + \\ 2\{\mathrm{V}'''_{\mathrm{Al}}{:}\mathrm{Al}^{\cdot}_{\mathrm{Mg}}\}'' + 4\{\mathrm{V}^{\cdot\cdot}_{\mathrm{O}}{:}\mathrm{Mg}'_{\mathrm{Al}}\}^{\cdot} + \mathrm{MgAl_2O_4} \end{aligned} \tag{4.40}$$

and in the case of the aluminium vacancies/interstitials for tetramer clusters:

$$3\mathrm{Mg}'_{\mathrm{Al}} + 3\mathrm{Al}^{\cdot}_{\mathrm{Mg}} + \mathrm{Al}^{\times}_{Al} \rightleftharpoons \{\mathrm{Al}^{\cdot\cdot\cdot}_{\mathrm{i}}{:}3\mathrm{Mg}'_{\mathrm{Al}}\}^{\times} + \{\mathrm{V}'''_{\mathrm{Al}}{:}3\mathrm{Al}^{\cdot}_{\mathrm{Mg}}\}^{\times} \tag{4.41}$$

Table 4.6 lists the intrinsic defect process energies as a function of clustering level. The picture at the trimer level of clustering is qualitatively similar to that for isolated defects with the Schottky and oxygen Frenkel the dominant

processes. In contrast to the isolated case the Mg Frenkel process is significantly higher in energy than the Schottky and the oxygen Frenkel processes. The clustered energies are throughout significantly lower than for isolated defects, the effect of this on overall defect concentration will be discussed in the following section where the mass action treatment of section 4.2.1 is revised to include the trimer clusters.

In addition to the antisite containing clusters discussed above, a range of vacancy and interstitial dimers might also be present in defective spinel. Table 4.7 comprises a list of potential dimer clusters, their associated formation energies and the cluster binding energies. As with the calculations in section 4.2.1 these have been repeated with and without shells on the O^{2-} ions. As in the previous section for each cluster all first and second neighbour configurations were investigated, where a second neighbour configuration was lower in energy the binding energies for third neighbour configurations were also studied.

Though table 4.7 shows all vacancy clusters $\{V_{\ddot{O}}:V''_{Mg}\}^{\times}$ and $\{V_{\ddot{O}}:V'''_{Al}\}'$ to have large binding energies, the loss of configurational entropy is such, however, that at the dilute limit, the Schottky energy is lower assuming isolated defects as opposed to clustered vacancies, as shown in table 4.8. Similarly the predicted energies for the 'partial Schottky' reactions (in table 4.9) are not lower assuming vacancy cluster formation than for the isolated defect case.

Table 4.6: Normalised energies for pseudo-equilibrium intrinsic defect processes, assuming both isolated and clustered defects, with and without shells and that antisites are already present in the lattice such that the antisite formation energy does not contribute the the defect process energies.

Process & clustering	Energy (shells)	Energy (no shells)
Mg Frenkel		
Isolated (eqn. 4.6)	5.46	6.19
Dimer clusters (eqn. 4.37)	4.57	5.15
Trimer clusters (eqn. 4.33)	3.69	4.57
Al Frenkel		
Isolated (eqn. 4.7)	6.93	7.54
Dimer clusters (eqn. 4.38)	5.48	5.83
Trimer clusters (eqn. 4.34)	3.81	4.47
Tetramer clusters (eqn. 4.41)	3.89	tba
O Frenkel		
Isolated (eqn. 4.8)	5.50	6.25
Dimer clusters (eqn. 4.39	3.86	4.15
Trimer clusters (eqn. 4.35)	2.91	3.14
Schottky		
Isolated (eqn. 4.9)	5.32	5.99
Dimer clusters (eqn. 4.40)	3.93	4.31
Trimer clusters (eqn. 4.36)	2.90	3.50

Table 4.7: Cluster defect and binding energies (BE) (eV), with and without shells. Positive binding energy equates to a bound cluster.

Cluster	Energy (shells)	BE (shells)	Energy	BE
$\{Mg_i^{\cdot\cdot}:O_i''\}^{\times}$	-31.70	-1.91	-30.88	-2.17
$\{Al_i^{\cdot\cdot\cdot}:O_i''\}^{\cdot}$	-60.17	-3.53	-60.34	-5.44
$\{Mg_i^{\cdot\cdot}:Al_{Mg}^{\cdot}:O_i''\}^{\cdot}$	-60.17	-3.53	-60.34	-5.44
$\{V_O^{\cdot\cdot}:V_{Mg}''\}^{\times}$	47.64	-4.06	49.00	-4.57
$\{V_O^{\cdot\cdot}:V_{Al}'''\}'$	76.82	-4.67	77.13	-5.35
$\{Mg_i^{\cdot\cdot}:V_{Al}'''\}'$	37.80	-2.91	37.80	-3.48
$\{Al_i^{\cdot\cdot\cdot}:V_{Mg}''\}^{\cdot}$	-17.76	-1.83	-16.00	-2.18
$\{Mg_{Al}':Al_{Mg}^{\cdot}\}^{\times}$	0.98	-0.48	0.94	-0.60

Table 4.8: Normalised defect process energies (eV), clustered defects, with and without shells.

Process	Energy (shells)	Energy (no shells)
Schottky	5.961	6.66
Cation antisite	0.98	0.94
$Mg_i^{\cdot\cdot} + V_{Al}''' + Al_{Mg}^{\cdot}$	3.09	3.13
$Al_i^{\cdot\cdot\cdot} + V_{Mg}'' + Mg_{Al}'$	4.07	4.65

Table 4.9: Normalised defect process energies for MgO and Al_2O_3 formation, clustered defects, with and without shells.

Process	Energy (shells)	Energy (no shells)
MgO formation	6.46	7.82
Al_2O_3 formation	5.99	6.37

Mass Action Calculations

Table 4.6 shows that the intrinsic defect process energies fall when it is assumed that the vacancy and interstitial defects form clusters with existing charge compensating antisite defects. This assumes that the antisite defects are available, the total formation energies to form the clusters from the perfect lattice is greater by 0.73 eV, when the shell model is used for oxygen and 0.77 eV when it is excluded. Even when this is added on, however, it is clear that in each case the trimer cluster's formation energy is lower than the corresponding dimer, which is in turn lower than the corresponding isolated process energy.

In section 4.2.1 mass action analysis was used to evaluate the relative defect concentrations of isolated intrinsic defects in $MgAl_2O_4$. This analysis can, in principle be extended to cover all possible defect equilibria, however due to the difficulty of simultaneously solving for many unknowns the results presented here include only the isolated and trimer defects. In addition to the mass action equations accounting for the formation of the isolated defects (equations 4.23-4.29) further equations are needed to govern the formation/dissolution of each trimer cluster. The defect equilibria are:

$$V''_{Mg} + 2Al^{\cdot}_{Mg} \rightleftharpoons \{V''_{Mg}{:}2Al^{\cdot}_{Mg}\}^{\times} \tag{4.42}$$

$$Mg^{\cdot\cdot}_{i} + 2Mg'_{Al} \rightleftharpoons \{Mg^{\cdot\cdot}_{i}{:}2Mg'_{Al}\}^{\times} \tag{4.43}$$

$$V'''_{Al} + 2Al^{\cdot}_{Mg} \rightleftharpoons \{V'''_{Al}{:}2Al^{\cdot}_{Mg}\}' \tag{4.44}$$

$$\mathrm{Al_i^{\cdots}} + 2\mathrm{Mg'_{Al}} \rightleftharpoons \{\mathrm{Al_i^{\cdots}}{:}2\mathrm{Mg'_{Al}}\}^{\cdot} \tag{4.45}$$

$$\mathrm{V_O^{\cdot\cdot}} + 2\mathrm{Mg'_{Al}} \rightleftharpoons \{\mathrm{V_O^{\cdot\cdot}}{:}2\mathrm{Mg'_{Al}}\}^{\times} \tag{4.46}$$

$$\mathrm{O_i''} + 2\mathrm{Al_{Mg}^{\cdot}} \rightleftharpoons \{\mathrm{O_i''}{:}2\mathrm{Al_{Mg}^{\cdot}}\}^{\times} \tag{4.47}$$

Which have the corresponding mass action equations:

$$\frac{[\{\mathrm{V''_{Mg}}{:}2\mathrm{Al_{Mg}^{\cdot}}\}^{\times}]}{[\mathrm{V''_{Mg}}][\mathrm{Al_{Mg}^{\cdot}}]^2} = \exp\left(\frac{-H_{eqn4.42}}{kT}\right) \tag{4.48}$$

$$\frac{[\{\mathrm{Mg_i^{\cdot\cdot}}{:}2\mathrm{Mg'_{Al}}\}^{\times}]}{[\mathrm{Mg_i^{\cdot\cdot}}][\mathrm{Mg'_{Al}}]^2} = \exp\left(\frac{-H_{eqn4.43}}{kT}\right) \tag{4.49}$$

$$\frac{[\{\mathrm{V'''_{Al}}{:}2\mathrm{Al_{Mg}^{\cdot}}\}']}{[\mathrm{V'''_{Mg}}][\mathrm{Al_{Mg}^{\cdot}}]^2} = \exp\left(\frac{-H_{eqn4.44}}{kT}\right) \tag{4.50}$$

$$\frac{[\{\mathrm{Al_i^{\cdots}}{:}2\mathrm{Mg'_{Al}}\}^{\cdot}]}{[\mathrm{Al_i^{\cdots}}][\mathrm{Mg'_{Al}}]^2} = \exp\left(\frac{-H_{eqn4.45}}{kT}\right) \tag{4.51}$$

$$\frac{[\{\mathrm{V_O^{\cdot\cdot}}{:}2\mathrm{Mg'_{Al}}\}^{\times}]}{[\mathrm{V_O^{\cdot\cdot}}][\mathrm{Mg'_{Al}}]^2} = \exp\left(\frac{-H_{eqn4.46}}{kT}\right) \tag{4.52}$$

$$\frac{[\{\mathrm{O_i''}{:}2\mathrm{Al_{Mg}^{\cdot}}\}^{\times}]}{[\mathrm{O_i''}][\mathrm{Al_{Mg}^{\cdot}}]^2} = \exp\left(\frac{-H_{eqn4.47}}{kT}\right) \tag{4.53}$$

The charge transfer equation, $\mathrm{Z}^+ \equiv \mathrm{Z}^-$, is also complicated by the introduction of the trimer cluster, the left hand side is now:

$$\mathrm{Z}^+ = 3[\mathrm{Al_i^{\cdots}}] + 2[\mathrm{Mg_i^{\cdot\cdot}}] + 2[\mathrm{V_O^{\cdot\cdot}}] + [\{\mathrm{Al_i^{\cdots}}{:}2\mathrm{Mg'_{Al}}\}^{\cdot}] + [\mathrm{Al_{Mg}^{\cdot}}] \tag{4.54}$$

and the right hand side:

$$Z^- = 3[V'''_{Al}] + 2[V''_{Mg}] + 2[O''_i] + [\{V'''_{Al}{:}2Al^{\cdot}_{Mg}\}'] + [Mg'_{Al}] \tag{4.55}$$

Finally, in order to ensure stoichiometric vacancy production, an analog of equation 4.32 must be used as a constraint:

$$\begin{aligned}
&([V^{\cdot\cdot}_O] + [\{V^{\cdot\cdot}_O{:}2Mg'_{Al}\}^{\times}]) - ([O''_i] + [\{O''_i{:}2Al^{\cdot}_{Mg}\}^{\times}]) = \\
&\frac{4}{3}\{([V'''_{Al}] + [\{V'''_{Al}{:}2Al^{\cdot}_{Mg}\}'] + [V''_{Mg}] + [\{V''_{Mg}{:}2Al^{\cdot}_{Mg}\}^{\times}]) \\
&-([Al^{\cdot\cdot\cdot}_i] + [\{Al^{\cdot\cdot\cdot}_i{:}2Mg'_{Al}\}^{\cdot}] + [Mg^{\cdot\cdot}_i] + [\{Mg^{\cdot\cdot}_i{:}2Mg'_{Al}\}^{\times}])\}
\end{aligned} \tag{4.56}$$

Solving these fifteen equations in the same temperature range as in figure 4.4 produces the results displayed in figure 4.5. The impact of clustering is significant: whereas in the isolated case the highest concentration predicted for vacancy/interstitial defects is $\sim 10^{-13}$; when clustering is taken into account this rises to $\sim 10^{-10}$. The assumption that the vacancies/interstitials are clustered is also supported: at its smallest, the difference between the concentration of clustered and unclustered states for a particular defect (V''_{Mg}) is an order of magnitude, where it is greatest ($V^{\cdot\cdot}_O$) the clustered defect concentration is 8 orders of magnitude higher than for the corresponding isolated defect. As with the isolated defect case no one species clearly dominates, although $V^{\cdot\cdot}_O$ defects are the most frequent, the difference in concentration between those and V'''_{Al} and O''_i is less than an order of magnitude.

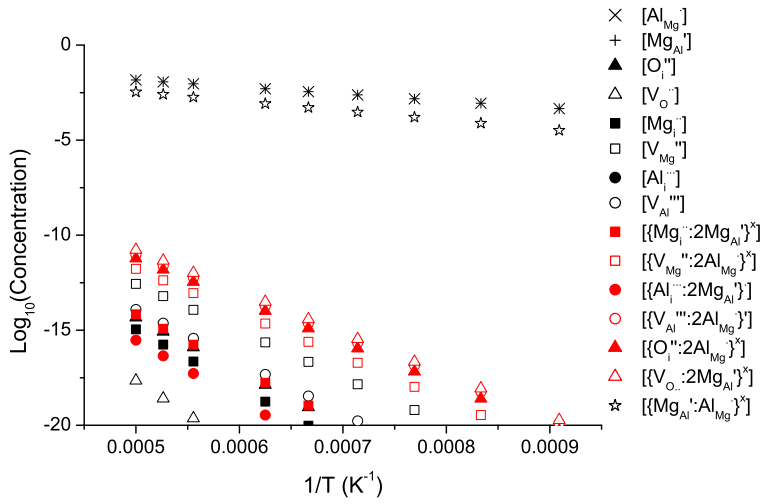

Figure 4.5: Intrinsic defect concentrations for $MgAl_2O_4$ spinel for temperatures in the range 1000K-2000K. Including isolated defects and trimer clusters.

4.3 Summary

Though $MgAl_2O_4$ is typically described as a normal spinel, i.e. all the Mg ions are occupy tetrahedral sites and Al ions octahedral sites, previous simulations [97] and experimental data [34] indicate a propensity to accommodate a degree of inversion on the cation lattice. It is thus unsurprising that formation of such antisite defects, via equation 4.1, is found to be the dominant intrinsic process. The presence in the lattice of a high concentration of antisite defects is predicted to have significant impact upon the equilibrium defect concentrations. Mass action calculations find that almost all vacancy and interstitial defects will, at equilibrium, be clustered with charge compensating defects. Exempting the antisite reaction, the Schottky and oxygen

Frenkel processes are lowest in energy and thus give rise to the most common defect species.